Vol. 26 • No. 35 • September 17 • 2014

www.advmat.de

ADVANCED MATERIALS

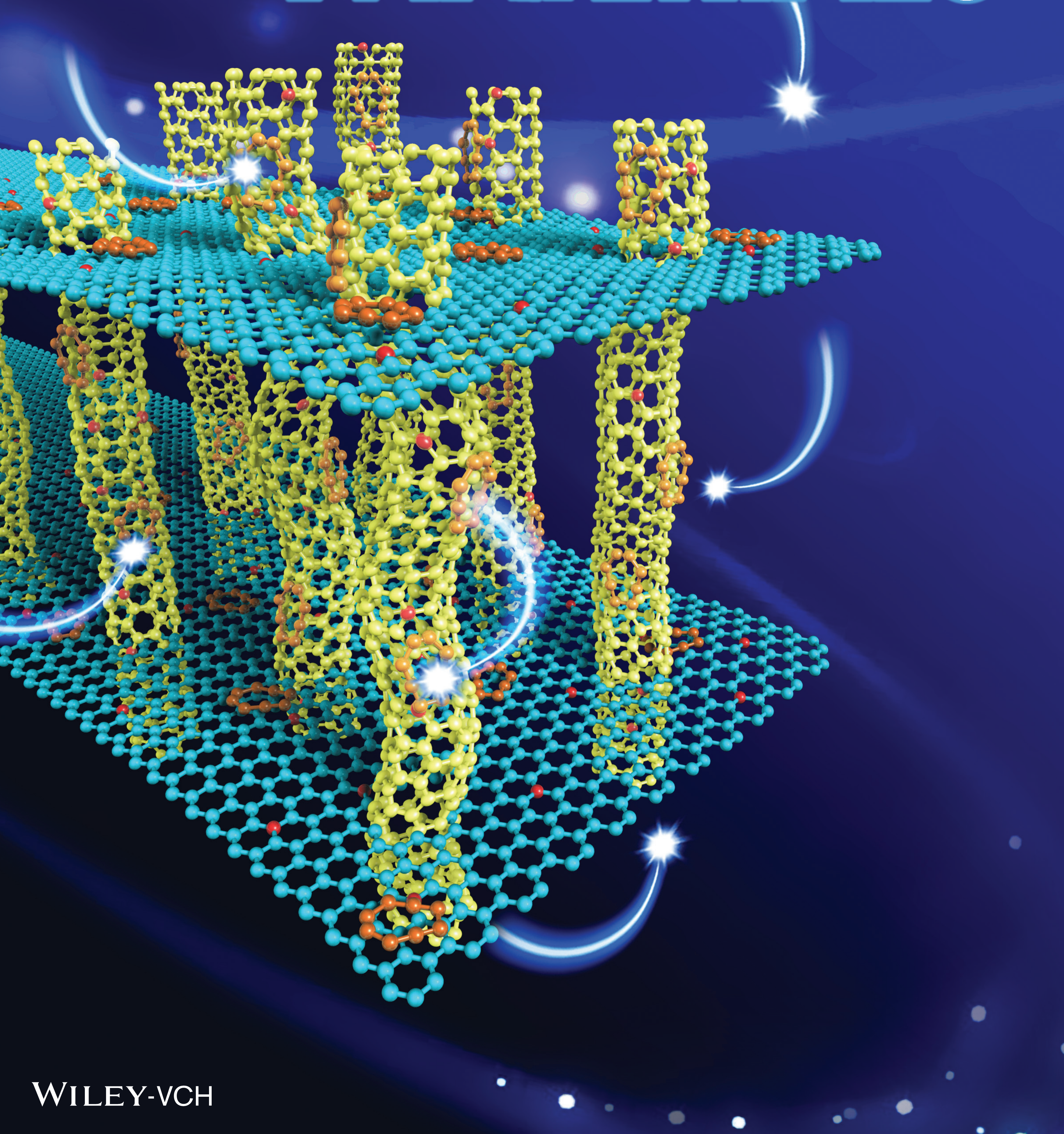

WILEY-VCH

ADVANCED MATERIALS
www.advmat.de

Materials Views
www.MaterialsViews.com

Nitrogen-Doped Aligned Carbon Nanotube/Graphene Sandwiches: Facile Catalytic Growth on Bifunctional Natural Catalysts and Their Applications as Scaffolds for High-Rate Lithium-Sulfur Batteries

Cheng Tang, Qiang Zhang, Meng-Qiang Zhao, Jia-Qi Huang, Xin-Bing Cheng, Gui-Li Tian, Hong-Jie Peng, and Fei Wei**

The broad applications of sp^2 carbon (e.g., carbon nanotubes (CNTs) and graphene) in the area of energy storage, heterogeneous catalysis, healthcare, environmental protection, as well as nanocomposites are highly dependent not only on their superior intrinsic physical properties, such as mechanical strength, electrical and thermal conductivity,[1] but also on their tunable chemical characters, such as functional groups, doping, and surface modification.[2] On one aspect, to fully demonstrate the remarkable inherent physical properties, a large number of rationally structured nanocomposites derived from CNTs and graphene (such as vertically aligned CNTs (ACNTs),[3] CNT sponges,[4] graphene foams,[5] graphene nanofibers,[6,7] unstacked double-layer graphene,[8] aerographite,[9] CNT or/and graphene-based films,[10–12] and aerogels,[13] etc.) have already been precisely designed and fabricated, rendering excellent performances from nanoscale to macroscale devices. On the other aspect, the chemical properties of sp^2 carbon nanomaterials have been easily tailored by heteroatom functionalization on nanocarbon sheets or molecular carbon geometries at the edges, defects, or strained regions, etc.[2] The incorporation of heteroatoms into the sp^2 carbon renders the induced modified carbon with significantly improved electrochemical performances and catalytic activities.[14]

However, the heteroatom-containing nanocarbon inclines to agglomerate due to strong van der Waals interactions and large surface area explosion. The CNTs prefer to form bundles and graphene sheets are easily to be packed with each other, which in turn constantly limits the demonstration of their intrinsic physical properties and performances in as-fabricated materials and practical devices. If the CNTs were effectively bonded with graphene, three-dimensional (3D) hierarchical composites that mitigate the self-aggregation and re-stacking of nanocarbon materials and also facilitate physical properties at macroscale can be fabricated.[15] A novel 3D carbon-network with alternate connections of aligned CNTs and graphene nanosheets was proposed as a new prototype,[16] and have triggered tremendous attention due to its extraordinary storage,[16] transport,[11,17] and mechanical performances.[11] The effective combination of CNTs and graphene can not only inherit full advantages of both CNTs and graphene, but also herald a new multifunctional nanostructured material with unexpected properties.[18,19] Up to now, several strategies have been explored to fabricate such aligned CNT/graphene (ACNT/G) hybrids, while it is still rare for facile integration of high-quality aligned CNTs and graphene without barrier layers, which hindered the full demonstration of the inherent excellent properties of the as-fabricated ACNT/G hybrids.[15,18,20]

Generally, the formation of ACNT/G hybrid was usually available via catalytic growth of one building block on the other one. However, the stability of metal catalysts on the carbon supports is very complex and metal-oxide barriers are commonly required during the synthesis. In this contribution, a metal-embedded supported bifunctional catalyst was proposed for the in-situ growth of ACNT/G sandwiches, with the metal nanoparticles as catalysts for CNT formation and metal-oxide lamellar as hard template catalyst for graphene deposition. To fully demonstrate the sp^2 carbon hybrids for energy storage, the chemical characters of carbon scaffolds were also modified via nitrogen incorporation for the formation of nitrogen-doped aligned CNT/graphene (N-ACNT/G) hybrid, as illustrated in **Figure 1**. The reason why we selected nitrogen as the dopant atoms is that nitrogen is a unique element that bears five valence electrons and induces a shift in the Fermi level to the conducting band, which affords the as-obtained carbon with curved microstructure, tunable interface, as well as improved reactivity.[21,22] The as-obtained N-ACNT/G was used as a 3D scaffold to accommodate sulfur for high-rate lithium-sulfur (Li-S) battery.

The vermiculite support consisting of metal oxides afforded catalytic activity[6,8,12,23] for graphene deposition at high temperature, and the metal catalysts reduced on vermiculite were with high density for aligned CNT formation.[3] In detail, exfoliated vermiculites impregnated with Fe/Mo were used as bifunctional catalysts for the in situ growth of aligned CNTs at 750 °C under C_2H_4 flow, and graphene deposition at 950 °C in CH_4 atmosphere sequentially. Parallel graphene sheets are pillared apart by vertically linked aligned CNTs, leading to a 3D

C. Tang, Prof. Q. Zhang, Dr. M.-Q. Zhao,
Dr. J.-Q. Huang, X.-B. Cheng, G.-L. Tian,
H.-J. Peng, Prof. F. Wei
Beijing Key Laboratory of Green Chemical
Reaction Engineering and Technology
Department of Chemical Engineering
Tsinghua University
Beijing 100084, P. R. China
E-mail: zhang-qiang@mails.tsinghua.edu.cn; wf-dce@tsinghua.edu.cn

DOI: 10.1002/adma.201401243

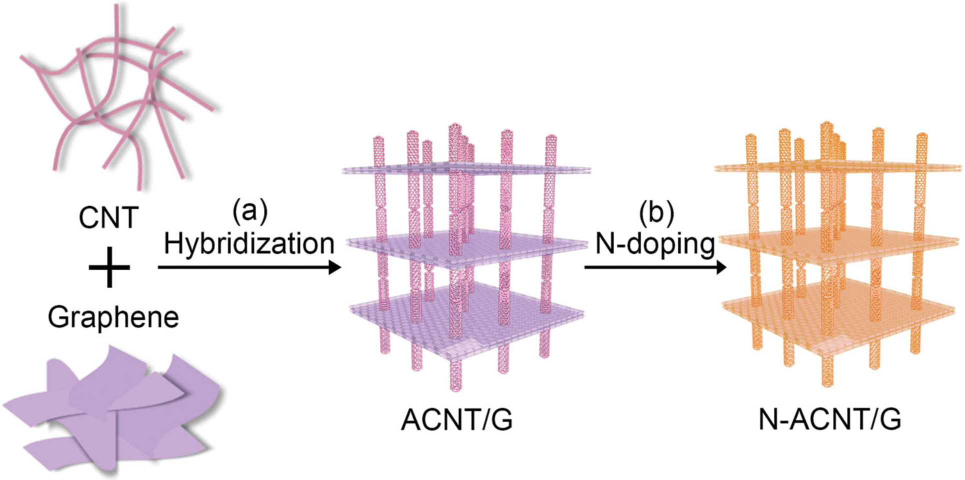

Figure 1. Conceptual scheme of the design of N-ACNT/G hybrids with graphene and aligned CNTs as building blocks. (a) Structural hybridization of aligned CNTs and graphene via catalytic growth on bifunctional natural catalysts; (b) In situ nitrogen doping for moderate chemical modification of the carbon scaffolds.

freestanding porous network (Figure 1a). NH_3 was simultaneously introduced during the CVD growth for the incorporation of nitrogen atoms into the carbon framework (Figure 1b). N-ACNT/G hybrids with a high purity of 98.3 wt.% were available after the removal of catalysts (Figure S1). ACNT/G hybrids grown on the same catalysts without NH_3 introduction for nitrogen-doping and ACNTs without the procedure of graphene deposition were prepared as control samples. The scanning electron microscopy (SEM) image (**Figure 2**a) revealed the typical sandwich-like structure of as-obtained hybrid, with aligned CNTs and graphene sheets grown vertically to each other, which was in long-range periodicity (Figure S2a). After a growth time of 30 min, the aligned CNTs grown from the vermiculite layers were uniform with a length of ca. 10 μm, which further expanded the adjacent vermiculite flakes, thereby giving rise to effective diffusion pathways for carbon source to infiltrate and reach the vermiculite layer for graphene deposition at the bottom of aligend CNT arrays. The top-view SEM and transmission electron microscopy (TEM) images clearly demonstrated the formation and effective link of graphene layers to the bottom of aligned CNTs (Figure S2b, 2b). Figure S2c further showed the connection region between aligned CNTs and

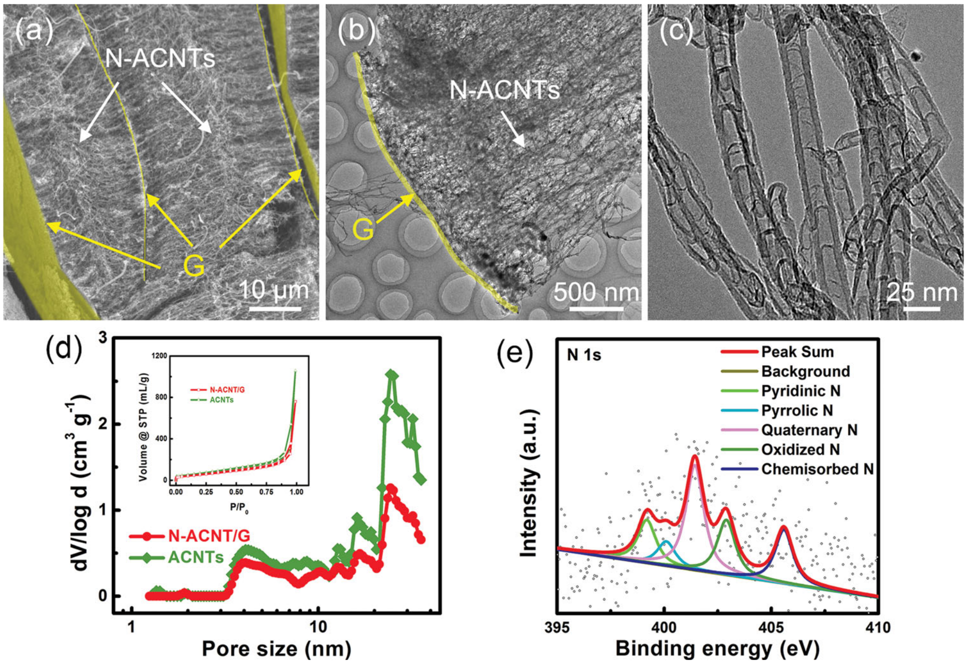

Figure 2. Structure characterization of N-ACNT/G hybrids. (a) SEM and (b) TEM images of N-ACNT/G hybrids; (c) Typical TEM image of the bamboo-structured NCNT in the hybrids; (d) The N_2 sorption isotherms (inset) and pore size distribution of N-ACNT/G hybrids and ACNTs based on QSDFT model; (e) The N 1s XPS spectra of N-ACNT/G hybrids.

graphene. There were about 2-4 graphene layers after 30 min deposition (Inset of Figure S2c). The typical bamboo-like structure of nitrogen-doped CNTs shown in Figure 2c revealed the successful doping of nitrogen atoms into the carbon scaffolds[24] and a moderate modification of the surface characters. Raman spectroscopy was employed to differentiate the crystalline structure of carbon after nitrogen doping (Figure S3). Both ACNTs and N-ACNT/G exhibited a disorder-induced D-band (~1350 cm^{-1}) caused by phonon scattering at defect sites or impurities, and a doubly degenerated G-band (~1580 cm^{-1}) assigned to in-plane vibration of sp^2 carbon.[25] The I_D/I_G ratio of N-ACNT/G hybrids (1.95) was much larger than that of ACNTs (0.99), demonstrating a relatively low graphitization degree and a higher density of defect sites due to the structural hybridization and nitrogen doping. The strong single-sharp 2D band around 2700 cm^{-1} arising from a double resonance process also revealed the few-layered characteristic of the as-grown graphene (Figure S3).[25]

The N_2 sorption isotherms of N-ACNT/G hybrids were similar to that of ACNTs (Inset of Figure 2d). Both the samples displayed hierarchical porous structures, which were mainly attributed to the high-order arrangement of aligned CNTs (Figure 2d). With the introduction of graphene sheets to the bottom of aligned CNTs, the self-aggregation of CNTs and the re-stacking of graphene in N-ANCT/G hybrids were supposed to be mitigated. However, the N-ACNT/G exhibited a relatively lower specific surface area (SSA) (217 $\text{m}^2\ \text{g}^{-1}$) than the ACNTs (259 $\text{m}^2\ \text{g}^{-1}$), and the total pore volume was decreased from 0.77 to 0.72 $\text{cm}^3\ \text{g}^{-1}$, which was attributed to the enhanced interfacial interaction and stacking due to the abundant functional groups on the surface of N-ACNT/G. The surface chemistry of N-ACNT/G hybrids was further evaluated by X-ray photoelectron spectroscopy (XPS). Both N 1s and O 1s peaks were observed besides the C 1s region, demonstrating that the carbon matrix was chemically modified with diverse functional groups (Figure S4). The nitrogen content was ca. 0.86 at.%, and various nitrogen bonding states had been distinguished (pyridinic N, pyrrolic N, quaternary N, oxidized N, and chemisorbed N) from high-resolution N 1s spectrum (Figure 2e, Table S1),[26] which were believed to tune the properties of carbon matrix with enhanced surface wettability and activity.[22,27] With the hybridization of 1D CNTs and 2D graphene and nitrogen modulation of the carbon matrix, the N-ACNT/G hybrids were expected to have robust structural stability, hierarchically connected ion pathway, 3D electron freeway, and enhanced surface affinity and activity, thereby rendering them as prospective alternates for effective electrochemical energy storage.

Herein, lithium-sulfur batteries were constructed based on N-ACNT/G@S composite cathodes, with ACNT/G@S and ACNT@S as control samples, to evaluate the electrochemical performance and elucidate the roles of hybridization and nitrogen doping. Lithium-sulfur batteries are with very high theoretical energy density of 2600 Wh kg^{-1}, and element sulfur is highly abundant in nature, and environment friendly as well. Therefore, lithium-sulfur system is a promising candidate for next-generation power sources.[28] The introduction of 3D nanocarbon hybrids is an effective strategy to overcome the ultra-low conductivity of element sulfur and lithium sulfide.[29] The carbon@sulfur cathodes were prepared through a facile melt-diffusion method at 155 °C for 1.0 h. The as-prepared cathodes were denoted as N-ACNT/G@S, ACNT/G@S, and ACNT@S, respectively. The energy dispersive spectroscopy (EDS) mapping of N-ACNT/G@S demonstrated that the sulfur was distributed uniformly in the N-ACNT/G scaffolds (Figure S5). No obvious characteristic XRD peaks of sulfur were observed for carbon@S nanocomposites, which also indicated a uniform distribution of sulfur in the carbon matrix (Figure S6). Thermogravimetric analysis (TGA) results indicated that the weight-loss temperature of N-ACNT/G@S was higher than that of ACNT/G@S and ACNT@S (Figure S7), suggesting a promoted affinity and interaction between sulfur and N-ACNT/G. The sulfur contents of composite cathodes were measured to be as 52.6, 50.0, and 48.5 wt% for N-ACNT/G@S, ACNT/G@S, and ACNT@S, respectively.

The cyclic stabilities of the N-ACNT/G@S, ACNT/G@S, and ACNT@S cathodes were tested at a current density of 1.0 C and illustrated in **Figure 3**a and S8a. The N-ACNT/G@S cathode showed a high initial discharge capacity of 1152 mAh g^{-1} based on sulfur, with nearly 76% capacity retention after 80 cycles (ca. 880 mAh g^{-1}). In contrast, the initial reversible capacity of ACNT@S cathode was 865 mAh g^{-1}, lower than that of N-ACNT/G@S by 25%, and only a capacity of 533 mAh g^{-1} was preserved after 80 cycles. Although ACNT/G@S cathode exhibited a slightly lower initial reversible capacity (764 mAh g^{-1}) than ACNT@S cathodes, a high capacity of 638 mAh g^{-1} was still available with a ultra-low cyclic fading rate of 0.2% for initial 80 cycles, indicating that the 3D sandwich-like architecture of aligned CNTs and graphene counted for the improved electrochemical stability. During the first 10 cycles, the cyclic fading rates of the initial capacity were ca. 0.3%, 0.3%, and 1.3% for N-ACNT/G@S, ACNT/G@S, and ACNT@S cathodes, respectively. The N-ACNT/G@S cathode exhibited both enhanced reversible capacity and electrochemical stability.

The rate performances of the Li-S batteries with N-ACNT/G@S and ACNT@S cathodes were illustrated as Figure 3b. With the current density varied from 0.2 to 5.0 C, the capacity decreased gradually due to the polarization effect. However, the N-ACNT/G@S cathodes exhibited much higher capacities than those of ACNT@S cathodes at all current densities. A reversible capacity of ca. 770 mAh g^{-1} can still be preserved at a very high current density of 5.0 C, indicating an excellent rate capability of the N-ACNT/G@S nanocomposites. The efficient connections between aligned CNTs and graphene layers constructed a novel 3D conductive network for rapid electron transfer along both horizontal and vertical directions, and an interconnected mesoporous architecture for improved electrolyte immersion and diffusion, thereby rendering the extraordinary rate performances. When returning to 0.2 C, the N-ACNT/G@S cathode still showed a high capacity of ca. 930 mAh g^{-1}.

For both N-ACNT/G@S and ACNT@S cathodes, two typical voltage plateaus at ca. 2.4 and 2.0 V were clearly observed from the galvanostatic discharge curves (Figure 3c). Generally, the capacity corresponding to the first plateaus at higher voltage is contributed by the reduction of S into high-order lithium polysulfides, indicating the effective utilization of active agents, and the capacity accumulated during the low-voltage plateaus is determined by the depth of further lithiation into lithium sulfide and/or lithium disulfide. Consequently, discharge

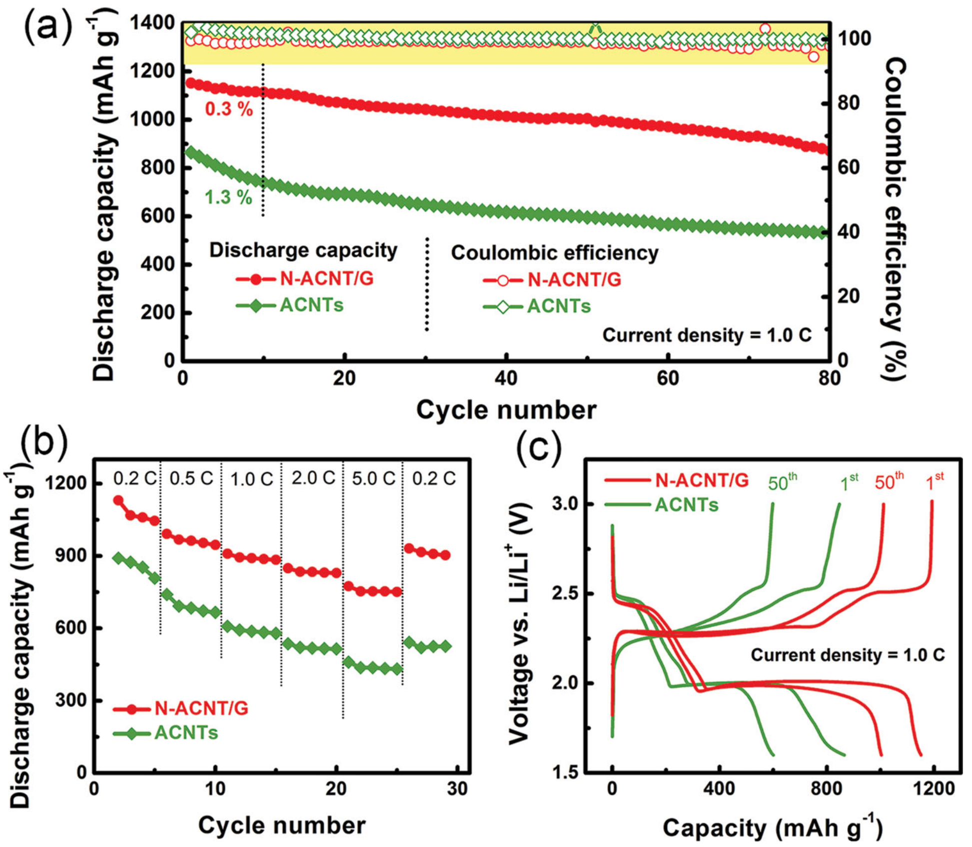

Figure 3. Electrochemical performance of N-ACNT/G hybrids and ACNTs for Li-S batteries. (a) The cycling performance at a current density of 1.0 C; (b) The rate performance; (c) The Galvanostatic charge-discharge curves at different cycles.

curves revealed the electrochemical behavior and mechanism. As shown in 4a, the N-ACNT/G@S cathodes exhibited much higher participation of sulfur than ACNT@S ones throughout the entire cycle calculated based on the discharge curves. Furthermore, the N-ACNT/G@S cathodes exhibited a stable lithiation degree around 1.60 while the degree of lithiation for ACNT@S cathodes was decreased from ca. 1.43 to 1.30 after 80 cycles, which exerted great influence on the reversible capacities (**Figure** 4b). For ACNT/G@S cathodes, in spite of a high degree of lithiation, the degree of sulfur participation was as low as ACNT@S, which accounted for the unsatisfactory reversible capacity (Figure S8b and S8c). The incorporation of nitrogen atoms into the hierarchical ACNT/G hybrids induced more active defect sites on the interface and edges, improving the affinity between sulfur, polysulfides and the nitrogen-doped carbon scaffolds,[22,27] thereby enhancing the utilization of sulfur and deep lithiation of polysulfides. These results imply the N-ACNT/G hybrids as very promising candidates for high-performance Li-S batteries, in aspects of the enhanced cycling capacity and rate capability, which can be ascribed to the following characteristics of the hybrids (Figure 4c and d): (1) the seamless junction of CVD-grown aligned CNTs and graphene for rapid electron transfer and mechanical robustness; (2) the 3D interconnected mesoporous space for easy penetration and diffusion of electrolytes; (3) the nitrogen-modified interfaces with enhanced interfacial affinity for efficient confinement and utilization of sulfur and polysulfides.

In summary, a rationally designed N-ACNT/G sandwich was proposed and fabricated via a two-step CVD growth. Aligned CNTs and graphene layers were in situ anchored to each other, constructing a sandwich-like hierarchical architecture with efficient 3D electron transfer pathways and ion diffusion channels. The moderate chemical modulation induced by nitrogen doping introduced more defects and active sites to the carbon framework, thereby improving the interfacial adsorption and electrochemical behaviors. When the novel N-ACNT/G hybrids were used as cathode materials for Li-S batteries, greatly enhanced cyclic and rate performances were demonstrated. A high initial reversible capacity of 1152 mAh g^{-1} can be available at 1.0 C, maintaining ca. 880 mAh g^{-1} after 80 cycles, which was about 65% higher than that of ACNTs. Even at a high current density of 5.0 C, a reversible capacity of ca. 770 mAh g^{-1} can be achieved. Such design strategy is generally applicable, opening up fresh perspectives to novel advanced functional composites, especially interface-modified hierarchical nanocarbons for wide applications, such as lithium batteries, supercapacitors, sensors, catalysis, and hydrogen storage.

Experimental Section

Catalyst Preparation: The vermiculite mined in Lingshou, P. R. China, with a size of ca. 150 μm was served as the catalyst support. The exfoliated vermiculite (EV) was impregnated into an aqueous solution of

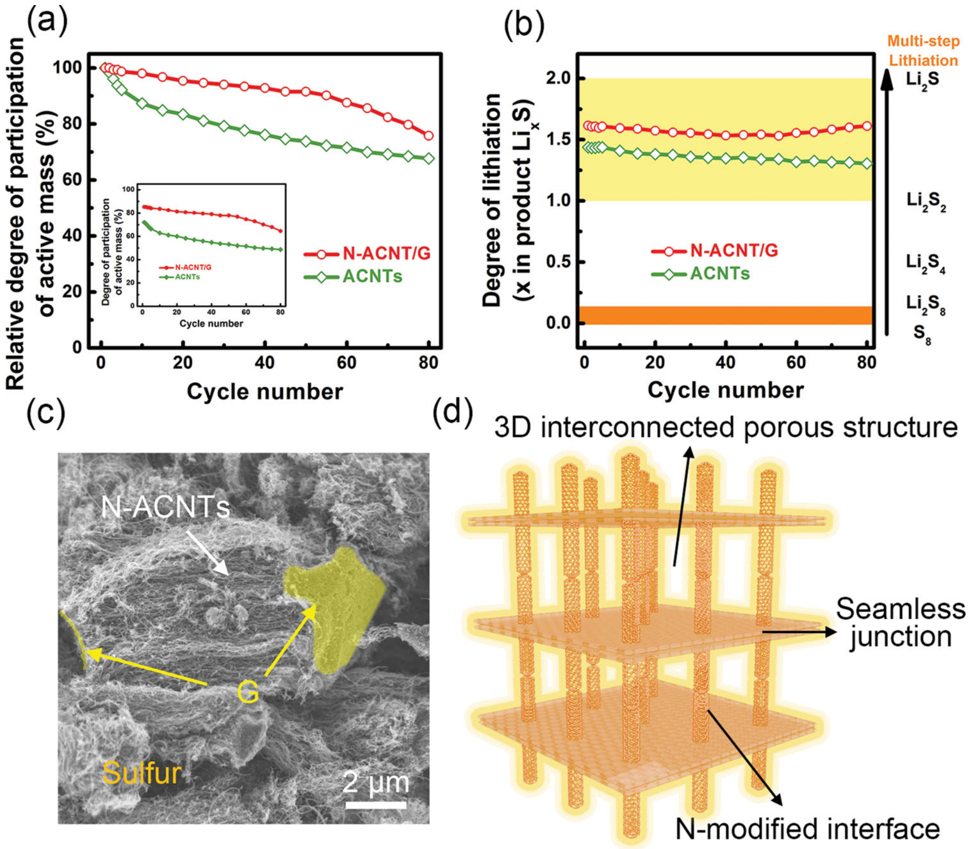

Figure 4. Electrochemical behaviors of N-ACNT/G@S and ACNT@S composite cathodes. (a) The participation percentage of active sulfur and (b) degree of lithiation during the initial 80 cycles; (c) SEM image and (d) illustration of N-ACNT/G@S composite.

$Fe(NO_3)_3{\cdot}9H_2O$ (>99.0 %) and $(NH_4)_6Mo_7O_{24}{\cdot}4H_2O$ (>99.0 %) with a Fe/Mo/EV mass ratio of 3 : 2 : 95 for 1.0 h at 80 °C, and then dried at 110 °C for 12.0 h, followed by washing, filtration, and drying. The as-prepared catalyst was employed for the growth of N-ACNT/G, ACNT/G hybrids, and ACNTs.

Synthesis of N-ACNT/G, ACNT/G Hybrids and ACNTs: The growth of nanocarbon materials underwent a typical chemical vapor deposition (CVD) operated in a horizontal quartz tube inserted into a furnace at atmospheric pressure. The FeMo/EV catalyst was sprayed uniformly onto a quartz boat and then placed at the center of the quartz tube. For N-ACNT/G hybrids, the reactor was firstly heated to 750 °C under a mixture of Ar (150 mL min^{-1}) and H_2 (120 mL min^{-1}), then C_2H_4 (60 mL min^{-1}) and NH_3 (50 mL min^{-1}) was introduced for 30 min for the intercalation of N-ACNT among EV flakes. After that, the tube was further heated to 950 °C in Ar atmosphere (150 mL min^{-1}), followed by graphene deposition at 950 °C for 30 min within an atmosphere of Ar (150 mL min^{-1}) and CH_4 (120 mL min^{-1}). ACNT/G hybrids were obtained without NH_3 introduction during the same growth process. To obtain ACNTs, only C_2H_4 (120 mL min^{-1}) was introduced on reaching 750 °C, and the growth time was tuned to make the length of the aligned CNTs similar to that of N-ACNT/G hybrids. After cooling down under Ar flow, the as-obtained products were treated with a HCl (6.0 mol L^{-1}) aqueous solution at 80 °C for 12.0 h and a HF (6.0 mol L^{-1}) aqueous solution at 80 °C for another 12.0 h to remove the catalyst. The N-ACNT/G, ACNT/G hybrids, and ACNTs were collected and characterized.

Fabrication of Carbon@sulfur Composite Cathodes: The carbon@sulfur composite cathodes were fabricated following a typical melt-diffusion strategy. The nanocarbon materials (N-ACNT/G, ACNT/G or ACNTs) were firstly mixed with sulfur powder with a mass ratio of 5 : 6 by milling. Subsequently, the mixture was placed in a sealed flask at 155 °C for 1.0 h to incorporate sulfur into the nanocarbon matrix. The loading capability of sulfur in the cathodes was about 1.0 mg cm^{-2}.

Characterizations: The morphology of the samples was characterized by a JSM 7401F (JEOL Ltd., Tokyo, Japan) SEM operated at 3.0 kV and a JEM 2010 (JEOL Ltd., Tokyo, Japan) TEM operated at 120.0 kV. Energy dispersive spectroscopy (EDS) analysis was performed at the acceleration voltage of 120.0 kV using a JEM 2010 (JEOL Ltd., Tokyo, Japan) TEM equipped with an Oxford Instrument energy dispersive spectrometer. The purity of the hybrids was obtained through thermalgravimetric analysis (TGA) by a TGA/DSC1 STAR^e system under O_2 flow, while the sulfur content of the cathode was measured under N_2 flow. The N_2 adsorption-desorption isotherm was collected using an Autosorb-IQ2-MP-C system. The specific surface area was calculated by the multipoint Brunauer–Emmett–Teller (BET) method, and the pore-size distribution was calculated based on Quenched Solid Density Function Theory (QSDFT). X-ray photoelectron spectroscopy (XPS) measurements were carried out by Escalab 250xi. X-ray diffraction (XRD) patterns were recorded on a Bruker D8 Advance diffractometer at 40.0 kV and 120 mA with Cu-K_α radiation.

Electrochemical Measurements: Two-electrode cells using standard 2025 coil-type cells were constructed to evaluate the electrochemical performance of the N-ACNT/G, ACNT/G hybrids or ACNTs as cathode materials for Li-S batteries. The cathode slurry was prepared by mixing 85% of the carbon@sulfur composites and 15% of the poly(vinylidene fluoride) binder in a *N*-methyl-pyrrolidone (NMP) solvent dispersant. The positive electrodes were fabricated through coating the slurry on aluminum foil and drying at 60 °C for 6.0 hr. A 0.5 mol/L lithium nitrate ($LiNO_3$) solution in tetraethylene glycol dimethyl ether (TEGDME) was used as electrolyte for electrochemical evaluation, with the exception that a 1.0 mol/L lithium bis(trifluoromethanesulfonyl)imide (LiTFSI) solution in 1:1 (v/v) 1,3-dioxolane/1,2-dimethoxyethane (DOL/DME) was used for rate capabilities. 50 μL electrolyte was used to construct each Li-S cell. Lithium metal foil was used as the anode and the polypropylene membranes from Celgard Inc. were used as the separators. The coin cells were tested in galvanostatic mode at various currents within a voltage range of 1.6–3.0 V using Neware multichannel battery cycler. A current density of 1672 mA g^{-1} (1.0 C) equivalent to full discharge or charge in one hour was applied in both current sweep directions. The capacities were calculated corresponding to the mass of sulfur in the cathodes.

Supporting Information

Supporting Information is available from the Wiley Online Library or from the author.

Acknowledgements

This work was supported by National Basic Research Program of China (973 Program, 2011CB932602) and Natural Scientific Foundation of China (No. 21306102, 21306103).

Received: March 19, 2014
Revised: April 12, 2014

---

[1] a) M. F. L. De Volder, S. H. Tawfick, R. H. Baughman, A. J. Hart, *Science* **2013**, *339*, 535; b) Q. Zhang, J.-Q. Huang, W.-Z. Qian, Y.-Y. Zhang, F. Wei, *Small* **2013**, *9*, 1237; c) U. N. Maiti, W. J. Lee, J. M. Lee, Y. Oh, J. Y. Kim, J. E. Kim, J. Shim, T. H. Han, S. O. Kim, *Adv. Mater.* **2014**, *26*, 40; d) Z. Y. Yin, J. X. Zhu, Q. Y. He, X. H. Cao, C. Tan, H. Y. Chen, Q. Y. Yan, H. Zhang, *Adv. Energy Mater.* **2014**, *4*, 1300574; e) X. Huang, X. Qi, F. Boey, H. Zhang, *Chem. Soc. Rev.* **2012**, *41*, 666; f) X. Huang, Z. Yin, S. Wu, X. Qi, Q. He, Q. Zhang, Q. Yan, F. Boey, H. Zhang, *Small* **2011**, *7*, 1876.

[2] a) L. Song, Z. Liu, A. L. M. Reddy, N. T. Narayanan, J. Taha-Tijerina, J. Peng, G. H. Gao, J. Lou, R. Vajtai, P. M. Ajayan, *Adv. Mater.* **2012**, *24*, 4878; b) J. P. Paraknowitsch, A. Thomas, *Energy Environ. Sci.* **2013**, *6*, 2839; c) D.-W. Wang, D. Su, *Energy Environ. Sci.* **2014**, *7*, 576.

[3] a) Q. Zhang, M. Zhao, Y. Liu, A. Cao, W. Qian, Y. Lu, F. Wei, *Adv. Mater.* **2009**, *21*, 2876; b) Q. Zhang, M.-Q. Zhao, J.-Q. Huang, Y. Liu, Y. Wang, W.-Z. Qian, F. Wei, *Carbon* **2009**, *47*, 2600.

[4] a) X. Gui, J. Wei, K. Wang, A. Cao, H. Zhu, Y. Jia, Q. Shu, D. Wu, *Adv. Mater.* **2010**, *22*, 617; b) X. Gui, Z. Zeng, Y. Zhu, H. Li, Z. Lin, Q. Gan, R. Xiang, A. Cao, Z. Tang, *Adv. Mater.* **2014**, *26*, 1248.

[5] a) X. Huang, K. Qian, J. Yang, J. Zhang, L. Li, C. Yu, D. Zhao, *Adv. Mater.* **2012**, *24*, 4419; b) Z. Niu, J. Chen, H. H. Hng, J. Ma, X. Chen, *Adv. Mater.* **2012**, *24*, 4144; c) Y. Long, C. Zhang, X. Wang, J. Gao, W. Wang, Y. Liu, *J. Mater. Chem.* **2011**, *21*, 13934; d) E. Singh, Z. Chen, F. Houshmand, W. Ren, Y. Peles, H.-M. Cheng, N. Koratkar, *Small* **2013**, *9*, 75; e) H. Hu, Z. B. Zhao, W. B. Wan, Y. Gogotsi, J. S. Qiu, *Adv. Mater.* **2013**, *25*, 2219; f) X. Cao, Y. Shi, W. Shi, G. Lu, X. Huang, Q. Yan, Q. Zhang, H. Zhang, *Small* **2011**, *7*, 3163.

[6] C. Cui, W. Qian, Y. Yu, C. Kong, B. Yu, L. Xiang, F. Wei, *J. Am. Chem. Soc.* **2014**, *136*, 2256.

[7] Z. L. Dong, C. C. Jiang, H. H. Cheng, Y. Zhao, G. Q. Shi, L. Jiang, L. T. Qu, *Adv. Mater.* **2012**, *24*, 1856.

[8] M.-Q. Zhao, Q. Zhang, J.-Q. Huang, G.-L. Tian, J.-Q. Nie, H.-J. Peng, F. Wei, *Nat. Comm.* **2014**, *5*, 3410.

[9] M. Mecklenburg, A. Schuchardt, Y. K. Mishra, S. Kaps, R. Adelung, A. Lotnyk, L. Kienle, K. Schulte, *Adv. Mater.* **2012**, *24*, 3486.

[10] a) Q. Zheng, B. Zhang, X. Lin, X. Shen, N. Yousefi, Z.-D. Huang, Z. Li, J.-K. Kim, *J. Mater. Chem.* **2012**, *22*, 25072; b) H. R. Byon, S. W. Lee, S. Chen, P. T. Hammond, Y. Shao-Horn, *Carbon* **2011**, *49*, 457.

[11] J. J. Shao, W. Lv, Q. Guo, C. Zhang, Q. Xu, Q. H. Yang, F. Kang, *Chem. Commun.* **2012**, *48*, 3706.

[12] G. Ning, C. Xu, Y. Cao, X. Zhu, Z. Jiang, Z. Fan, W. Qian, F. Wei, J. Gao, *J. Mater. Chem. A* **2013**, *1*, 408.

[13] M. A. Worsley, P. J. Pauzauskie, T. Y. Olson, J. Biener, J. H. Satcher Jr., T. F. Baumann, *J. Am. Chem. Soc.* **2010**, *132*, 14067.

[14] a) Z.-S. Wu, W. Ren, L. Xu, F. Li, H.-M. Cheng, *ACS Nano* **2011**, *5*, 5463; b) Y. Shao, S. Zhang, M. H. Engelhard, G. Li, G. Shao, Y. Wang, J. Liu, I. A. Aksay, Y. Lin, *J. Mater. Chem.* **2010**, *20*, 7491; c) P. Chen, T.-Y. Xiao, Y.-H. Qian, S.-S. Li, S.-H. Yu, *Adv. Mater.* **2013**, *25*, 3192.

[15] a) M.-Q. Zhao, X.-F. Liu, Q. Zhang, G.-L. Tian, J.-Q. Huang, W. Zhu, F. Wei, *ACS Nano* **2012**, *6*, 10759; b) M. Q. Zhao, Q. Zhang, J. Q. Huang, G. L. Tian, T. C. Chen, W. Z. Qian, F. Wei, *Carbon* **2013**, *54*, 403.

[16] G. K. Dimitrakakis, E. Tylianakis, G. E. Froudakis, *Nano Lett.* **2008**, *8*, 3166.

[17] F. D. Novaes, R. Rurali, P. Ordejon, *ACS Nano* **2010**, *4*, 7596.

[18] a) F. Du, D. Yu, L. Dai, S. Ganguli, V. Varshney, A. Roy, *Chem. Mater.* **2011**, *23*, 4810; b) Y. Zhu, L. Li, C. Zhang, G. Casillas, Z. Sun, Z. Yan, G. Ruan, Z. Peng, A.-R. O. Raji, C. Kittrell, R. H. Hauge, J. M. Tour, *Nat. Comm.* **2012**, *3*, 1225.

[19] a) W. Wang, S. Guo, M. Penchev, I. Ruiz, K. N. Bozhilov, D. Yan, M. Ozkan, C. S. Ozkan, *Nano Energy* **2013**, *2*, 294; b) W. Wang, I. Ruiz, S. Guo, Z. Favors, H. H. Bay, M. Ozkan, C. S. Ozkan, *Nano Energy* **2014**, *3*, 113; c) Y. Wu, T. Zhang, F. Zhang, Y. Wang, Y. Ma, Y. Huang, Y. Liu, Y. Chen, *Nano Energy* **2012**, *1*, 820; d) M. Q. Zhao, Q. Zhang, J. Q. Huang, F. Wei, *Adv. Funct. Mater.* **2012**, *22*, 675.

[20] Z. Fan, J. Yan, L. Zhi, Q. Zhang, T. Wei, J. Feng, M. Zhang, W. Qian, F. Wei, *Adv. Mater.* **2010**, *22*, 3723.

[21] a) X.-G. Sun, X. Wang, R. T. Mayes, S. Dai, *ChemSusChem* **2012**, *5*, 2079; b) L. Qie, W.-M. Chen, Z.-H. Wang, Q.-G. Shao, X. Li, L.-X. Yuan, X.-L. Hu, W.-X. Zhang, Y.-H. Huang, *Adv. Mater.* **2012**, *24*, 2047; c) L. Sun, C. Tian, Y. Fu, Y. Yang, J. Yin, L. Wang, H. Fu, *Chem. Eur. J.* **2014**, *20*, 564; d) F. Sun, J. Wang, H. Chen, W. Li, W. Qiao, D. Long, L. Ling, *ACS Appl. Mater. Interfaces* **2013**, *5*, 5630.

[22] a) W. H. Shin, H. M. Jeong, B. G. Kim, J. K. Kang, J. W. Choi, *Nano Lett.* **2012**, *12*, 2283; b) J. Song, T. Xu, M. L. Gordin, P. Zhu, D. Lv, Y.-B. Jiang, Y. Chen, Y. Duan, D. Wang, *Adv. Funct. Mater.* **2014**, *24*, 1243.

[23] S. Chen, J. Y. Bi, Y. Zhao, L. J. Yang, C. Zhang, Y. W. Ma, Q. Wu, X. Z. Wang, Z. Hu, *Adv. Mater.* **2012**, *24*, 5593.

[24] a) G. L. Tian, M. Q. Zhao, Q. Zhang, J. Q. Huang, F. Wei, *Carbon* **2012**, *50*, 5323; b) P. Ayala, R. Arenal, M. Rummeli, A. Rubio, T. Pichler, *Carbon* **2010**, *48*, 575.

[25] A. C. Ferrari, J. C. Meyer, V. Scardaci, C. Casiraghi, M. Lazzeri, F. Mauri, S. Piscanec, D. Jiang, K. S. Novoselov, S. Roth, A. K. Geim, *Phys. Rev. Lett.* **2006**, *97*, 187401.

[26] J.-Q. Huang, M.-Q. Zhao, Q. Zhang, J.-Q. Nie, L.-D. Yao, D. S. Su, F. Wei, *Catal. Today* **2012**, *186*, 83.

[27] Z. Wang, X. Niu, J. Xiao, C. Wang, J. Liu, F. Gao, *RSC Adv.* **2013**, *3*, 16775.

[28] a) Y. X. Yin, S. Xin, Y. G. Guo, L. J. Wan, *Angew. Chem. Int. Ed.* **2013**, *52*, 13186; b) A. Manthiram, Y. Z. Fu, Y. S. Su, *Accounts. Chem. Res.* **2013**, *46*, 1125.

[29] a) D. W. Wang, Q. C. Zeng, G. M. Zhou, L. C. Yin, F. Li, H. M. Cheng, I. R. Gentle, G. Q. M. Lu, *J. Mater. Chem. A* **2013**, *1*, 9382; b) Y. Yang, G. Zheng, Y. Cui, *Chem. Soc. Rev.* **2013**, *42*, 3018; c) R. Chen, T. Zhao, J. Lu, F. Wu, L. Li, J. Chen, G. Tan, Y. Ye, K. Amine, *Nano Lett.* **2013**, *13*, 4642; d) S. M. Zhang, Q. Zhang, J. Q. Huang, X. F. Liu, W. C. Zhu, M. Q. Zhao, W. Z. Qian, F. Wei, *Part. Part. Syst. Char.* **2013**, *30*, 158; e) G. M. Zhou, S. F. Pei, L. Li, D. W. Wang, S. G. Wang, K. Huang, L. C. Yin, F. Li, H. M. Cheng, *Adv. Mater.* **2014**, *26*, 625.